Behavioral and transcriptomic analyses of mecp2 function in zebrafish

Nicholas J. Santistevan[1,2,✉], **Colby T. Ford**[3,4,5], **Cole S. Gilsdorf**[1], **and Yevgenya Grinblat**[1,✉]

[1]University of Wisconsin – Madison, Departments of Integrative Biology and Neuroscience, Madison, WI, USA
[2]University of Wisconsin – Madison, Genetics Ph.D. Training Program, Madison, WI, USA
[3]University of North Carolina at Charlotte, School of Data Science, Charlotte, NC, USA
[4]University of North Carolina at Charlotte, Department of Bioinformatics and Genomics, Charlotte, NC, USA
[5]Tuple LLC, Charlotte, NC, USA

Rett Syndrome (RTT), a human neurodevelopmental disorder characterized by severe cognitive and motor impairments, is caused by dysfunction of the conserved transcriptional regulator Methyl-CpG-binding protein 2 (MECP2). Genetic analyses in mouse Mecp2 mutants, which exhibit key features of human RTT, have been essential for deciphering the mechanisms of MeCP2 function; nonetheless, our understanding of these complex mechanisms is incomplete. Zebrafish mecp2 mutants exhibit mild behavioral deficits but have not been analyzed in depth. Here we combine transcriptomic and behavioral assays to assess baseline and stimulus-evoked motor responses and sensory filtering in zebrafish mecp2 mutants from 5-7 days post-fertilization (dpf). We show that zebrafish mecp2 function is dispensable for gross movement, acoustic startle response, and sensory filtering (habituation and sensorimotor gating), and reveal a previously unknown role for mecp2 in behavioral responses to visual stimuli. RNA-seq analysis identified a large gene set that requires mecp2 function for correct transcription at 4 dpf, and pathway analysis revealed several pathways that require MeCP2 function in both zebrafish and mammals. These findings show that MeCP2's function as a transcriptional regulator is conserved across vertebrates and supports using zebrafish to complement mouse modeling in elucidating these conserved mechanisms.

MeCP2 | zebrafish | transcriptomic analysis | Rett Syndrome (RTT) | behavioral analysis

Correspondence: ***nsantistevan@wisc.edu (NJS); ygrinblat@wisc.edu (YG)***

Introduction

Methyl-CpG-binding protein 2 (*MECP2*) is an X-linked, transcriptional regulatory gene associated with a number of disorders marked by cognitive impairment, including autism, schizophrenia, and attention-deficit hyperactivity disorder (1–3). Mutations in *MECP2* are causally linked to Rett Syndrome (RTT), a neurodevelopmental disorder that affects 1̃ in 10,000-20,000 girls and is characterized by cognitive defects, impaired motor coordination, loss of language skills and hand use, and seizures (4–6). Patients with RTT exhibit normal postnatal development for the first 6-18 months of life, followed by developmental stagnation and a rapid regression of motor and cognitive function (5). RTT patients present with reductions in brain volume, neuronal soma size and dendritic arborization, and immature synaptic connections (7).

Animal models of MeCP2 dysfunction have been critical to understanding the role of MeCP2 in neurodevelopment, cognitive and motor function, and transcriptional regulation. MeCP2 is conserved across vertebrates, with the transcriptional regulatory (TRD) and methyl-binding domains (MBD) sharing strong amino acid identity between humans, mice, and zebrafish (8). In mice, brain-specific deletions of *Mecp2* cause neuronal aberrations similar to those observed in RTT patients, including impaired synaptic physiology, impaired dendritic morphogenesis (9, 10), and motor and cognitive deficits typical of RTT (11–17). Similarly, *mecp2*^{Q63X} homozygous zebrafish, which harbor a predicted loss-of-function mutation, exhibit decreased thigmotactic responses, decreased activity, and mild motor dysfunction in response to mechanical stimulation (18).

Zebrafish is a powerful model system for exploring how MeCP2 functions in the brain to control distinct aspects of behavior. *mecp2* is expressed broadly in the zebrafish embryo, including the brain, as early as 24-48 hours post-fertilization (hpf) (8, 19). Its expression at this early time point is notable as the circuits that mediate several stereotyped behaviors develop between 24 and 96 hours and begin to function immediately thereafter (20, 21). Here we used a two-pronged approach to ask how *mecp2* functions in zebrafish: behavioral assessment and transcriptomic (RNA-seq) analysis. Using a panel of assays to quantify the initiation, execution, and modulation of several baseline and stimulus-evoked behaviors, we show largely normal baseline behaviors and normal measures of sensory filtering (acoustic habituation and prepulse inhibition (PPI)), in 5 days post-fertilization (dpf) *mecp2* mutant zebrafish. Notably, *mecp2* mutant zebrafish showed an aberrant response to visual stimuli that has not been reported in mouse mutants.

In many tissues and molecular pathways, MeCP2 functions as a methyl-binding transcription factor that acts as both a transcriptional activator and a repressor (22, 23). Our RNA-Seq analysis of 4 dpf *mecp2* mutants identified a large set of genes that require *mecp2* function for correct transcription, and pathway analysis showed enrichment of several pathways previously associated with Rett syndrome, indicative of a deep conservation of MeCP2 functions in vertebrates. Collectively, these results suggest that zebrafish is a useful, yet under-utilized model system that could provide valuable insights into the function of MeCP2, contributing to our understanding of neurodevelopmental disorders associated with MeCP2 dysfunction.

Results

mecp2 mutant zebrafish show normal spontaneous locomotion. Patients with RTT and mouse models of MeCP2 dysfunction exhibit impaired mobility. To evaluate motor function in *mecp2*^{Q63X} homozygous mutant zebrafish, which harbor a predicted loss-of-function mutation (18), we assessed 5-7 dpf larval zebrafish for baseline activity levels, kinematics, and their responses to various stimulus paradigms. We first quantified baseline activity in *mecp2* mutant larvae by measuring gross movement over time and the frequency of spontaneous initiation of a turn or swim maneuver. To do this, we recorded 6 dpf *mecp2* mutant larvae and wild-type siblings for 3 minutes and measured several aspects of their swimming behaviors, namely, distance moved, initiations of turns, and initiations of swimming bouts. Over the 3-minute recording period, *mecp2* mutant and wild-type siblings showed similar gross movement with no difference in the distance swam (Fig. 1A). Next, we divided the 3-minute recording window into 30 second intervals and assessed larvae for turn initiations and swimming bouts during each interval. Across the recording window, *mecp2* mutant and wild-type siblings exhibited similar probability of initiating turns (Fig. 1B; 6 recording intervals for both genotypes) and swimming bouts (Fig. 1C; 6 recording intervals for both genotypes). Together, these results indicate that 6 dpf *mecp2* mutants show normal baseline activity and normal locomotion. *mecp2* mutants show normal baseline activity and normal locomotion.

mecp2 mutants show normal sensory filtering of the acoustic startle response. Since loss of Mecp2 function in mice results in impaired acoustic startle response (ASR) (11, 24), we asked if loss of mecp2 function impaired acoustic startle behavior in larval zebrafish. By 5 dpf, zebrafish have established the neural circuits sufficient to control ASRs with kinematic parameters similar to those observed in adult zebrafish (25). The ASR is driven by the Mauthner hindbrain reticulospinal interneuron, the command neuron of the ASR (26). Each Mauthner neuron receives direct acoustic input from sensory hair cells via the VIIIth nerve (27). The Mauthner sends descending commissural axons down the spinal cord to stimulate contralaterally positioned motor neurons, which induces a contralateral trunk muscle contraction and results in the zebrafish turning away from the acoustic stimulus (26, 28–30) . To examine the initiation, performance, and modulation of ASR behavior in *mecp2* larvae, we used a semi-automated behavioral platform that delivers a series of acoustic stimuli at defined intensities and intervals, records ASRs with a high-speed camera, and tracks individual larvae's movement to quantify aspects of ASR behavior.

The circuit that drives the ASR in zebrafish exhibits experience-dependent modulation of the ASR, namely, habituation learning and sensorimotor gating (20). Habituation has been termed the simplest form of non-associative learning that is exhibited by all animals (31) and is observed as a progressive decline in responsiveness to repeated, insignificant stimuli. To explore the requirement for *mecp2* function in ASR modulation, we assessed habituation by administering 10 high-intensity acoustic stimuli at non-habituating intervals of 20 seconds, followed by 30 high-intensity acoustic stimuli at habituating intervals of 1.5s (Fig. 1D). Habituation was calculated by taking the ratio of responses to the habituating and non-habituating stimuli (Fig. 1E) (29). Analysis of habituation between *mecp2* mutant larvae and wild-type siblings revealed that *mecp2* mutant zebrafish habituate normally (Fig. 1F).

Next, we measured prepulse inhibition (PPI) of the ASR (20), a widely used measure of sensorimotor gating in animal models and humans (32), thought to specifically reflect the function of inhibitory microcircuits (33). PPI of the ASR measures the ability of a weak acoustic stimulus to attenuate an animal's responsiveness to a subsequently presented, strong acoustic stimulus (34). Larvae were exposed to a series of acoustic stimuli, including low intensity stimuli that rarely evoke an ASR, high intensity stimuli that typically cause an ASR, and paired stimuli to measure PPI, in which a low intensity stimulus was delivered 300 milliseconds preceding a high intensity stimulus (Fig. 1G). PPI percentage was calculated by taking the ratio of responses to the high of the paired stimuli over the responses to the high stimulus alone (Fig. 1H) (20). At each intensity level, acoustic startle was the same in *mecp2* mutants and wild-type siblings (Fig. 1I) indicative of normal PPI in *mecp2* mutants (Figure 1J).

mecp2 mutant zebrafish exhibit aberrant visually-guided behaviors. The visual system is emerging as a reliable biomarker of MeCP2 disruption with both mouse models and RTT patients displaying lowered visual acuity (35, 36). Conditional Mecp2 deletion in GABAergic parvalbumin-expressing cells has been shown to abolish experience-dependent critical period plasticity of visual circuits and impair visual acuity (37). To ask if mecp2 function is required for visual behaviors in zebrafish, we compared the initiation and execution of stereotyped visually-evoked behaviors in 5-7 dpf *mecp2* mutants. It is important to note these responses are not mediated by the Mauthner neuron and show kinematics that are distinct from the ASRs (25). Following adaptation to a given light intensity, zebrafish larvae perform a turning maneuver when exposed to a sudden increase in light ('light flash') or the abrupt absence of light ('dark flash') (25, 38, 39). Following exposure to light flashes, 7 dpf *mecp2* mutants showed an increased response frequency compared to wild-type siblings (Fig. 2A). Analysis of the kinematic properties of light flash evoked turns showed that *mecp2* mutants execute turn responses with a shorter mean initiation latency, i.e. faster (Fig. 2B). The mean angle turned while executing the light flash evoked turn was greater in *mecp2* mutants (Fig. 2C). The mean duration of the light flash evoked turn was also greater in *mecp2* mutants (Fig. 2D) but mean swim velocity was indistinguishable from wild-type siblings (Fig. 2E).

In response to an abrupt absence of light, or "dark flash", larval zebrafish execute an O-bend, characterized by a large angle turn in which they reorient their bodies by ~180 degrees (25, 38). We evaluated the probability of 5 dpf *mecp2*

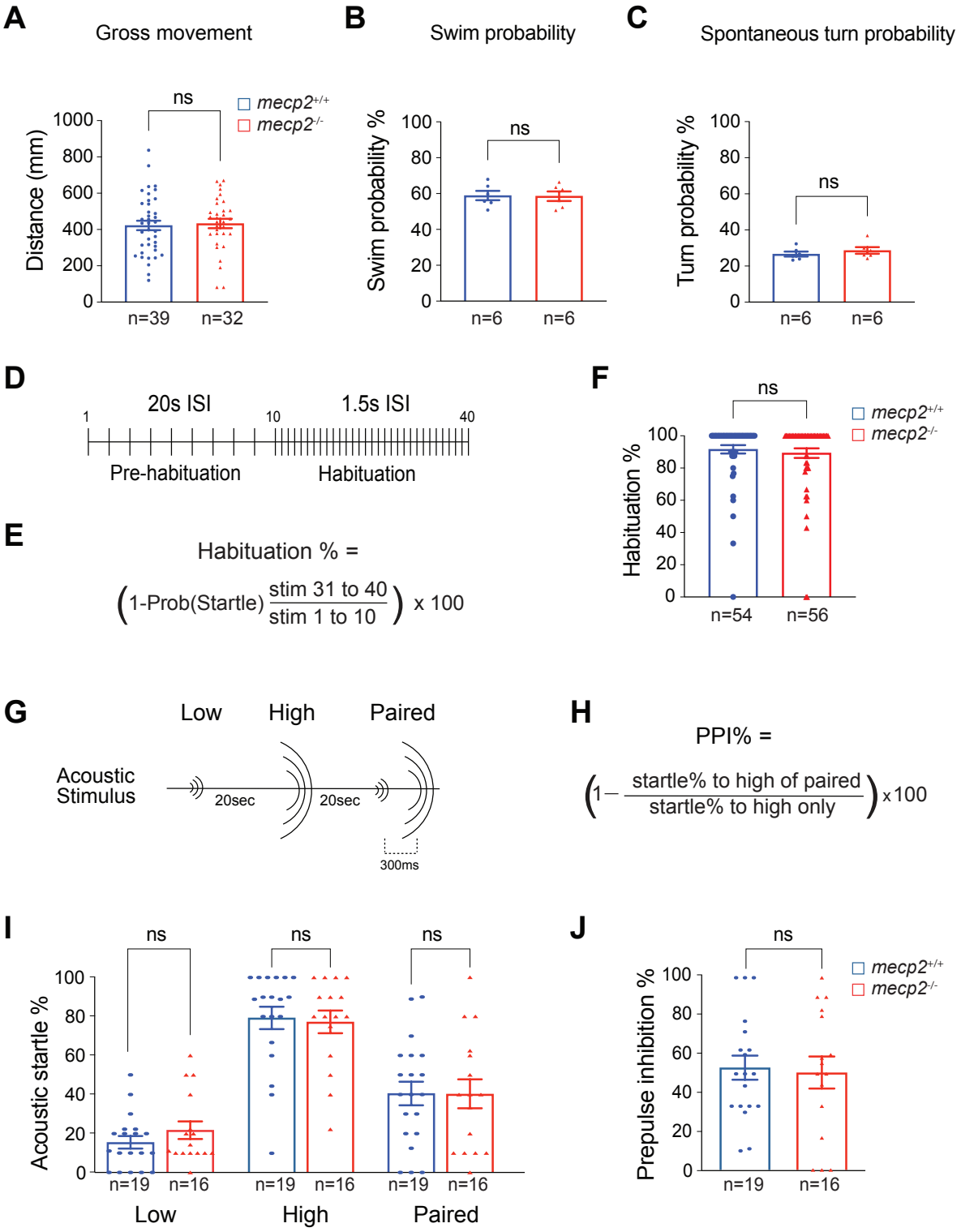

Fig. 1. *mecp2* mutants exhibit normal baseline activity and measures of sensory filtering. (A-C) Baseline motor activity levels between *mecp2* mutant larvae and wild-type siblings including overall gross movement (A), probability of initiating swimming bouts (B), and probability of initiating spontaneous turns (C). (D, E) Schematic representation of the habituation assay (D) and formula used to calculate habituation (E). Stimuli 1-10 were delivered at non-habituating 20s intervals and stimuli 11-40 were delivered at habituating 1.5s intervals. (F) Mean habituation of wild-type (shown in blue) and *mecp2* mutant (shown in red) larvae. Schematic representation of the prepulse inhibition (PPI) assay (G) and formula used to calculate PPI% (H). (I) Startle responsiveness of *mecp2* mutants and wild-type siblings to low, high, and paired acoustic stimuli. (J) Mean PPI% of *mecp2* mutants and wild-type siblings. Number of larvae shown at the bottom of the graphs. *p<0.05, **p<0.01,Mann-Whitney test versus wild-type. Mann-Whitney. Error bars denote SEM.

mutants to initiate an O-bend turn maneuver to dark flashes after the larvae had adapted to light and found a marked reduction in O-bend initiations in response to dark flashes (Fig 2F). Kinematic analysis of O-bend initiation showed an increase in mean latency to initiate the O-bend in mutants compared to wild-types (Fig 2G). The mean angle turned while performing the O-bend was also increased in *mecp2* mutants (Fig 2H) and the mean duration of the O-bend turn was markedly longer in *mecp2* mutants compared to wild-types at all dark flash intensities (Fig 2I) while mean swim velocity was indistinguishable between wild-types and mutants (Fig. 2J). Together, these results suggest a role for *mecp2* in mediating the detection or response to the light OFF and ON retinal pathways.

Transcriptomic analysis reveals conserved RTT-associated pathways in zebrafish. Next, we performed bulk RNA-Seq transcriptomic analysis comparing *mecp2* mutant larvae and wild-type siblings at 4 dpf, the earliest stage when the circuit that drives the acoustic startle response is both fully developed and fully functional. RNA was prepared from pools of 3 individual *mecp2* mutant embryos and pools of 3 age-matched wild-type embryos, with 10 replicates per genotype, reverse-transcribed and sequenced on the Illumina platform. Bioinformatic analysis, carried out as described in Materials and Methods, identified 2659 differentially expressed genes (DEGs) in *mecp2* mutant homozygotes (Benjamini-Hochberg corrected FDR <0.05); transcript levels were significantly up-regulated at 1,394 loci and down-regulated at 1,265 loci (Fig. 3A, Supplemental Table 1, see Supplementary Data in the GitHub repository).

We examined the DEGs for expression of two known MeCP2 target genes, NMDA receptors *bdnf* (40), and *creb1* (41), and found them unchanged in *mecp2* mutants. Expression levels of MeCP2 homologs *mbd1, mbd2*, *mbd3,* and *mbd4* were likewise either unchanged or decreased in *mecp2* mutants (*mbd1a*, fold decrease= -0.236, p value = 0.007) (Supplemental Table 1, see Supplementary Data in the GitHub repository).

Kyoto Encyclopedia of Genes and Genomes (KEGG) analysis and Gene Set Enrichment Analysis (GSEA) are bioinformatic tools used to analyze gene expression data and identify enriched biological pathways. KEGG is a comprehensive knowledge base that provides information on gene functions and molecular networks by mapping gene expression data onto the KEGG pathways to identify those that are significantly enriched with differentially expressed genes (42, 43). KEGG analysis of the DEG set revealed 7 pathways significantly affected in *mecp2* mutants, including the G2-M DNA damage checkpoint of the cell cycle and cholesterol homeostasis, among others (adjusted p value <0.05) (Table 1). Each of the 7 pathways identified in *mecp2* mutant zebrafish have also been reported in studies of Mecp2-deficient mouse models and/or patients with RTT (see Table 1 for citations). GSEA is a computational method that assesses whether a set of genes, defined by a biological pathway or a functional category, is enriched at the top or bottom of a ranked list of genes (44). We performed GSEA on the expression data and identified 14 molecular pathways that were activated and 26 that were suppressed (Fig. 3B) in the *mecp2* larvae (adjusted p value < 0.05). Among these, cholesterol homeostasis, which was suppressed in *mecp2* mutants, was of note as it was also identified in KEGG analysis and it has been demonstrated that cholesterol homeostasis is disrupted in *Mecp2* mutant mice (45) and is altered in cells derived from RTT patients (46).

Previous work in mice has shown that loss of Mecp2 function yields increased brain cholesterol concentration which has detrimental effects on neuron development and function due to perturbed cholesterol homeostasis (45, 50). The mevalonate pathway is responsible for the production of isoprenoids, which are essential for various cellular functions, including cholesterol synthesis (54), while the steroid biosynthesis pathway is involved in the catabolism and elimination of cholesterol (55). The mevalonate and steroid biosynthesis pathways work together to maintain cholesterol homeostasis in the body. Tracing the mevalonate-cholesterol pathway through defined KEGG pathways (dre:00900, dre:00100, and dre:00140) and overlaying mutant vs. wild-type expression of each gene exemplifies the changes in expression due to *mecp2* mutation (56) (Fig. 4). Specifically, both the mevalonate pathway and steroid biosynthesis pathways are activated in *mecp2* mutant zebrafish, leading to altered cholesterol synthesis.

Discussion

Impairments in sensorimotor gating of the ASR have been documented in Mecp2-deficient mouse models and in patients with RTT, and we asked if this aspect of MeCP2 function was conserved in a teleost model, the zebrafish. Using a panel of behavioral assays in *mecp2* mutants aged 5-7 days, we show that mecp2 function is dispensable for ASR, but is required for correct visually-guided startle responses in zebrafish. Genome-wide transcriptional analysis of *mecp2* mutants identified a large set of differentially expressed genes and several molecular pathways that require MeCP2 function in zebrafish and in mammals; these include glycolysis, the G2-M DNA damage checkpoint, and cholesterol homeostasis. This conservation, together with the unique advantages of zebrafish for high-throughput drug screening and long-term behavioral analysis, support the utility of the zebrafish model system for dissecting conserved mechanisms of MeCP2 function in vertebrates.

Modeling motor deficits associated with Rett Syndrome. Previous research has shown that mice with brain-specific deletions of Mecp2 exhibit impaired synaptic physiology and motor and cognitive deficits typical of RTT (9–11, 16, 57). These deficits include limited mobility, decreased motor coordination measured using rotarod assays, and decreased cognition measured using cued and conditional tasks, with deficits associated with learning and memory (13–15, 58, 59). A prior study found that *mecp2* mutation in zebrafish results in increased spontaneous contractions at 25 hpf and an increased duration of head tactile-

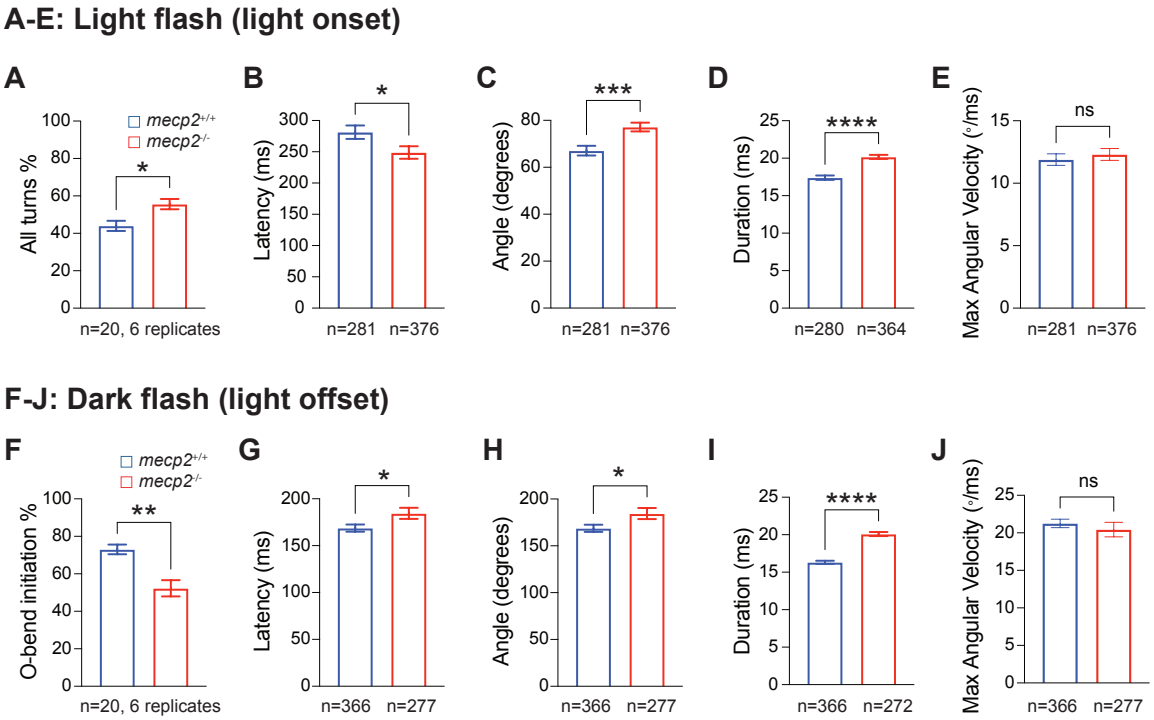

Fig. 2. *mecp2* mutants exhibit aberrant kinematic parameters and responses to light offset and light onset. (A) Light flash elicits a low angle turn response. Mean frequency of turns initiated to a series of 10 light flash stimuli. wild-type siblings are shown in blue and *mecp2* mutants are shown in red. *p<0.05, Mann-Whitney test versus wild-type. Number of larvae across 6 replicates shown at the bottom of graph. Error bars denote SEM. (B-E) Kinematic analysis of the light flash induced turning response including turn latency (B), turn angle (C), turn duration (D), and turn angular velocity (E). *p<0.05, ***p<0.001, ****p<0.0001. Mann-Whitney test versus wild-type. Number of responses measured shown at the bottom of graphs. Error bars denote SEM. (F) Dark flash elicits O-bend response. Mean frequency of O-bend responses initiated to a series of dark flash stimuli. wild-type siblings are shown in blue and *mecp2* mutants are shown in red. **p<0.01, Mann-Whitney test versus wild-type. Number of larvae across 6 replicates shown at the bottom of graph. Error bars denote SEM. (G-J) Kinematic analysis of the dark flash induced O-bend response including turn latency (G), turn angle (H), turn duration (I), and turn angular velocity (J). *p<0.05, ****p<0.0001, Mann-Whitney test versus wild-type. Number of responses measured shown at the bottom of graphs. Error bars denote SEM.

Pathway	adjusted *p*-value	Enrichment Score	Normalized Enrichment Score	Mouse Correlates	Human Correlates
Hallmark: G2M Checkpoint	0.01767409	-0.70082419	-2.293993545	Brunton et al. (2011)	
Hallmark: E2f Targets	0.01767409	-0.69856014	-2.286582663	Julian et al. (2015)	
Hallmark: Mitotic Spindle	0.01767409	-0.66985581	-2.192625395		Bergo et al. (2015)
Hallmark: Cholesterol Homeostasis	0.03746254	0.663982631	1.929031339	Nagy and Ackerman (2013)	Buchovecky et al. (2013); Segatto et al. (2014)
Hallmark: Unfolded Protein Response	0.03853565	0.580473281	1.795013601	Matagne et al. (2021)	
Hallmark: Myc Targets V2	0.04307251	0.650583804	1.826797434		Bernard et al. (2005)
Hallmark: Mtorc1 Signaling	0.04307251	0.486936897	1.611009807	Rangasamy et al. (2016)	

Table 1. Pathway analysis reveals conserved pathways between zebrafish, MECP2 mouse models, and RTT patients. KEGG analysis revealed several pathways affected by loss of *mecp2* in 4 dpf larval zebrafish. All pathways are conserved between *mecp2* mutant zebrafish, Mecp2-deficient mouse models, and/or patients with RTT. Pathways with adjusted *p* values <0.05 are shown. The full list of leading-edge genes with altered expression for each of these pathways is listed in Supplemental Table 2, see Supplementary Data in the GitHub repository.

evoked startle responses at 51 hpf (18), which may be indicative of an excitation/inhibition imbalance in *mecp2* mutants. This study also reported that loss-of-function mutation of *mecp2* in zebrafish larvae at 6 dpf leads to reduced thigmotaxis, decreased activity, and swimming bouts with lower velocity (18). Interestingly, morpholino-mediated knockdown of *mecp2* at 28 hpf and 72 hpf results in decreased motor activity, as measured by slower touch responses and abnormal/slower swimming, respectively (19). Our assessment of locomotor activity in 6 dpf *mecp2* mutant zebrafish indicate that *mecp2* function is dispensable for additional measures of baseline motor activity, as evidenced by normal overall gross movement, frequency of spontaneous swimming bouts, and frequency of spontaneous turns. Taken together, these analyses provide a comprehensive characterization of baseline activity in free-swimming 6 dpf *mecp2* mutant larvae.

Modeling cognitive deficits associated with Rett Syndrome. Impaired sensorimotor gating of the acoustic startle response has been observed in conditional *Mecp2* knockout mice (11) and disorders associated with MECP2 dysfunction (60–63). Unexpectedly, we found no impairments in experience-dependent modulation of the ASR in *mecp2* mutants, as both habituation learning and sensorimotor gating, measured by PPI, were normal. Importantly, there are discrepancies in how sensory filtering deficits manifest in humans with RTT and Mecp2-null mouse models. In RTT patients, sensorimotor gating is often reduced (32, 64), while in *Mecp2* knockout mice (both global and GABA neuron-specific) increased PPI has been observed (11, 65).

(A)

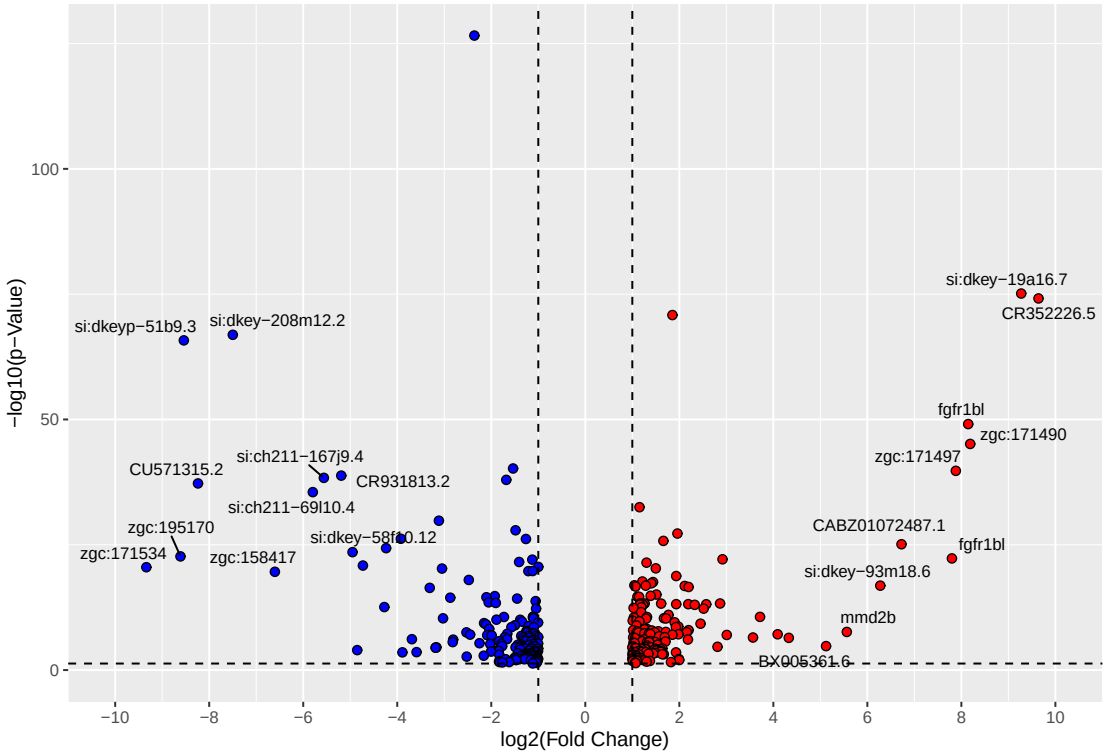

(B)

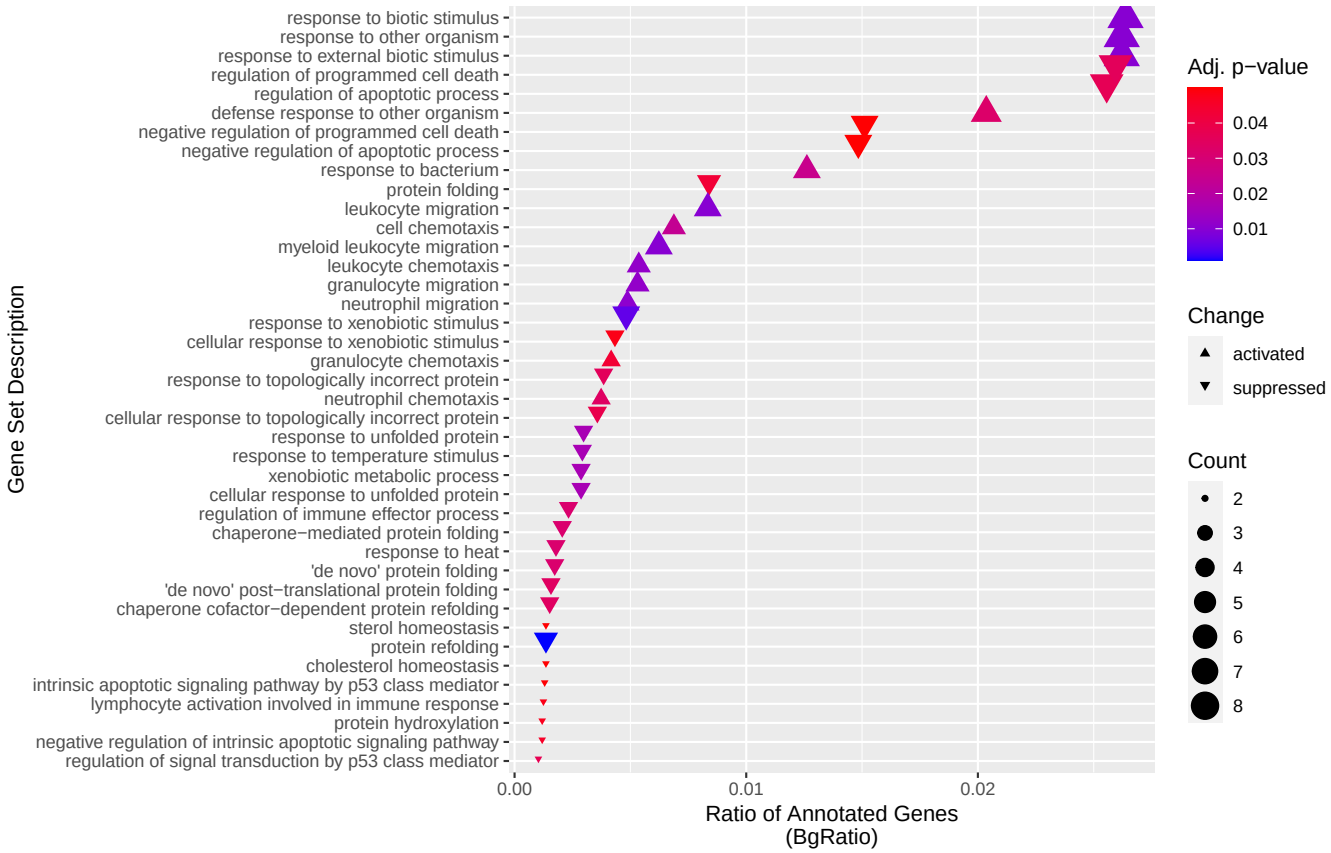

Fig. 3. Transcriptome analysis identifies activated and suppressed genes and gene sets in *mecp2* mutants. (A) A volcano plot depicting the fold change and statistical significance of individual genes, with $\log_2$(Fold Change) by -$\log_{10}$(p-value) of individual genes shown as points and colorized by their significance and change in regulation (grey is non-significant, red is significant and upregulated, blue is significant and downregulated). The names of top 10 upregulated genes and top 10 downregulated genes by $\log_2$(Fold Change) were labeled. (B) The top 40 differentially expressed gene sets in *mecp2* mutants relative to wild-type siblings, identified by GSEA, with 14 activated and 26 suppressed gene sets with adj. *p*-value < 0.05. This plot shows the BgRatio (the ratio of annotated genes) by gene set descriptor, points colored by the adjusted *p*-value, sized by count of genes in each set, and points shaped by the overall change (activated vs. suppressed).

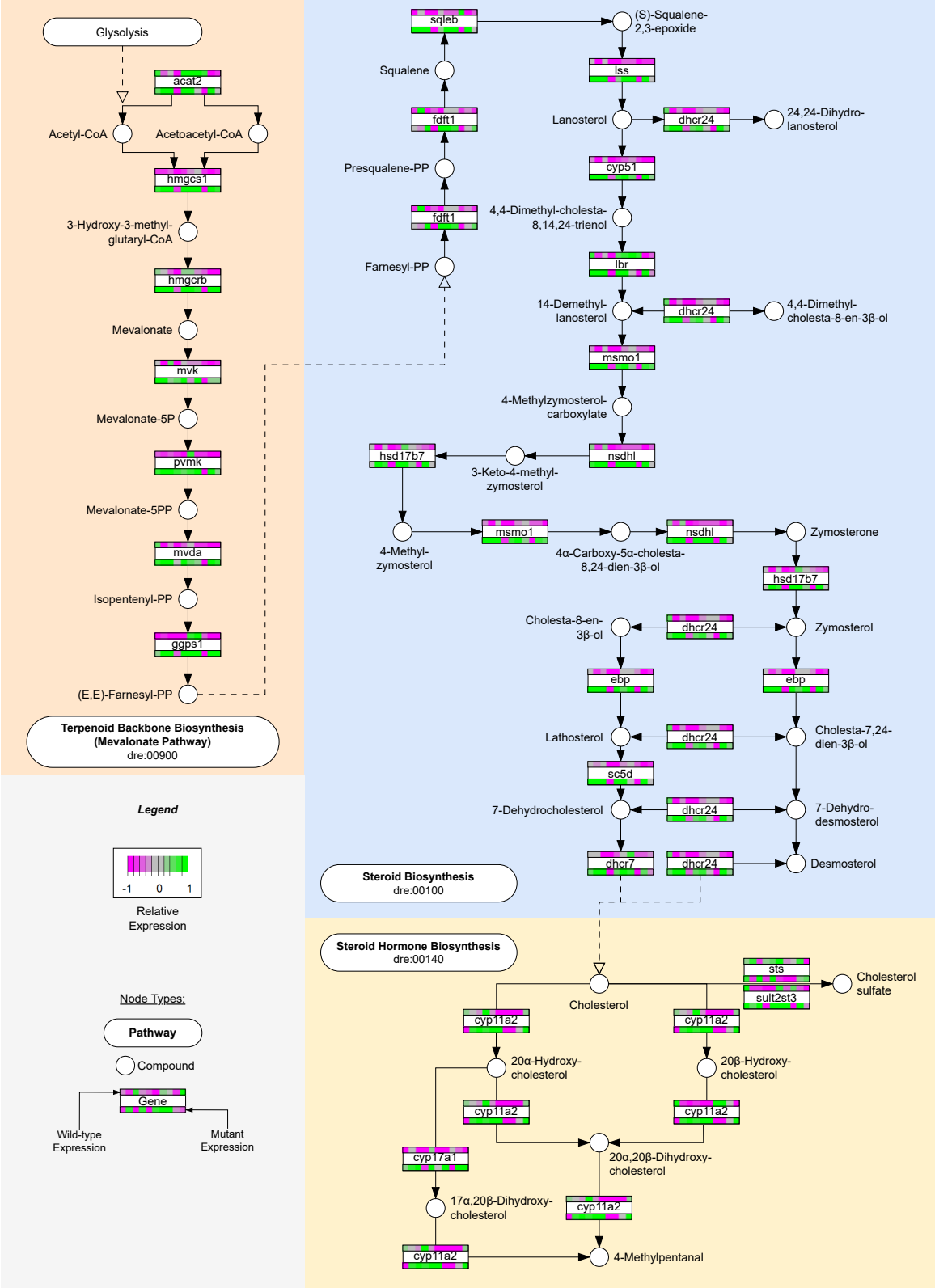

Fig. 4. Relative gene expression differences shown between *mecp2* mutants and wild-type siblings throughout the mevalonate-cholesterol pathway. A combined mevalonate-cholesterol pathway, simplified from KEGG pathways dre:00900, dre:00100, and dre:00140 to show only genes relevant to this study and *D. rerio*. Color bars on each gene node represent the relative gene expression of each sample in this study, scaled between [-1,1]. The top color bar of a given gene node represents the 10 wild-type samples and the bottom color bar represents the 10 mutant samples.

The discrepancy in PPI between the zebrafish and murine Mecp2 loss-of-function models may reflect differences in how PPI is measured in these models and/or the presence of additional behavioral deficits in the *Mecp2* knockout mice that could influence their PPI measures. In mice, the ASR is measured as a graded response to stimulus intensity, measured by the downward force applied to a testing platform when startled (66). PPI is evident when the force generated during an ASR to an intense stimulus preceded by a weak stimulus is less than that generated to an intense stimulus alone. In *Mecp2* knockout mice, reduced acoustic sensitivity and motor deficits (Chao et al., 2010; Ure et al., 2016) can generally diminish the ASR to high-intensity stimuli, indirectly leading to an enhanced PPI phenotype. While the zebrafish ASR shares kinematic and pharmacodynamic properties with mammalian ASR (20, 67), the zebrafish ASR is an all-or-nothing behavior, defined by the initiation of a "C-bend". PPI in zebrafish is indicated by a reduced probability of C-bend initiation to an intense stimulus that is preceded by a weak stimulus, compared to the probability of C-bend initiation to a high stimulus alone (Figs. 3D-3E) (20). Thus, PPI in zebrafish represents suppressed initiation while in mice it reflects a reduction in response intensity. Although the ASR circuitry in zebrafish is highly analogous to the mammalian ASR circuit, albeit simpler, there are likely differences that determine the all-or-nothing versus graded nature of their respective ASR and thus, may explain why PPI is altered in mice and humans, but not zebrafish, following MeCP2 dysfunction. Our study provides insights into the behavioral effects of *mecp2* mutation in zebrafish, highlighting potential species-specific differences in the function of MeCP2 on sensory filtering.

Modeling visually-guided behaviors. The visual processing and visual memory deficits observed in individuals with RTT (68), combined with the reduced visual acuity in both mouse models and RTT patients (35, 36), highlight the importance of assessing and addressing visual functioning in intervention strategies for RTT. Visual acuity measures are gaining recognition as reliable biomarkers of MeCP2 dysfunction (35, 36) and our study provides the first evidence that mecp2 plays a similar role in the zebrafish model. *mecp2* mutant zebrafish exhibit an enhanced light flash (light onset) response with distinct alterations in kinematic parameters and attenuated responses to dark flash (light offset) stimuli, accompanied by impaired kinematic parameters. These data show that mecp2 is important for the visual system that responds to changes in illumination, but do not distinguish between a requirement for light perception (visual acuity) and motor response circuitry. It is important to note these responses are not mediated by the Mauthner neuron and show kinematics that are distinct from the ASR (20).

Retinal photoreceptors are a likely site for mecp2 function in the visual system as these cells are able to distinguish between light offset and light onset stimuli. Their responses to these stimuli are driven by parallel circuits within the retina that are dependent on the modulation of glutamate release in cone-to-bipolar cell synapses (69). Increased synaptic vesicle release by cones activates OFF bipolar cells in response to light offset stimuli, while reduced synaptic vesicle release by cones activates ON bipolar cells in response to light onset stimuli (38). Taken together, these data suggest that analysis of the structure and function of the synapses between cones and discrete ON/OFF bipolar cell types will further elucidate the role of mecp2 in the visual circuit.

Prior research has indicated that light offset responses rely on insulin-like growth factor (IGF) signaling, which depends on proper cleavage of IGF binding proteins (IGFBPs) by proteases, enabling IGF to bind its receptor (Miller et al., 2018). Our transcriptomic analysis of *mecp2* mutant zebrafish revealed elevated expression of several IGFBP genes, suggesting reduced IGF availability and signaling (Supplemental Table 1, see Supplementary Data in the GitHub repository). Notably, IGF-1 has emerged as a promising therapeutic target for RTT patients, as exogenous IGF-1 supplementation has shown to ameliorate many RTT-like symptoms in *Mecp2* mutant mice (10, 70, 71). Taken together, these results highlight conserved functions of MeCP2 in the visual response pathway and indicate that MeCP2 dysfunction results in a disruption in detection and/or interpretation of changes in illumination, which may be due to dysregulation of photoreceptor synaptic development.

Molecular pathways regulated by mecp2. A previous study used transcriptomic analysis of zebrafish *mecp2* mutants to demonstrate enrichment of processes relevant to RTT phenotypes; however, this analysis was performed on 6-hpf early gastrula embryos (72) and well before the critical stages of neural circuit formation (24-96 hpf) in the zebrafish embryo (20, 21). We reasoned that RNAseq at 96 hpf (4 dpf) would capture *mecp2* targets that were most relevant to the circuits tested for function in our behavioral assays. Our analysis uncovered 2659 differentially expressed genes and identified multiple molecular pathways with distinct patterns of activation and suppression, including those involved in glycolysis, G2-M DNA damage checkpoint, and cholesterol homeostasis. Among these pathways, cholesterol homeostasis was of particular note since cholesterol metabolism alterations have been documented in RTT patients (46) and even minor disruptions of cholesterol metabolism in mice profoundly impact neuronal development and lead to neurological abnormalities, including impaired limb clasping and tremors (45, 50). Importantly, dysregulation of cholesterol homeostasis was also evident in the brain of *Mecp2*-deficient mice, and the administration of cholesterol-lowering statin drugs improved motor phenotypes and overall health and extended lifespan in *Mecp2* mutant mice (50). Collectively, these data support the exciting possibility that MeCP2 plays a conserved role in regulating cholesterol metabolism, offering a promising avenue for potential therapeutics targeting this pathway in addressing the impact of MeCP2 dysfunction on neurological function and development.

The unexpectedly mild phenotypes exhibited by *mecp2* mutants may be due to genetic compensation of MeCP2 homologs through transcriptional adaptation, a compensatory mechanism that increases transcription of genes that share

sequence similarity with a mutated gene (73, 74). While our transcriptome analysis of *mecp2* mutant zebrafish did not produce evidence of transcriptional upregulation of *mecp2* homologs *mbd1, mbd2*, *mbd3,* and *mbd4* at 4 dpf, it is possible that genetic compensation ameliorates the consequences of mecp2 dysfunction at other stages of development. Symptoms of RTT typically emerge in patients between 6-18 months of age, following a period of normal development marked by achievement of developmental milestones such as crawling or walking (5, 16). The decline in patients is progressive, with motor and cognitive symptoms manifesting in stages over time. Similarly, *Mecp2*-deficient mice exhibit normal development for the first 4 weeks, followed by a progressive deterioration of motor function (Vashi & Justice, 2019), resulting in impaired locomotion and premature death (61). By 7 weeks of age, mutant mice display enhanced PPI that persists into adulthood (57). Despite their behavioral and transcriptomic deficits, homozygous *mecp2* mutant zebrafish appear to develop normally to adulthood, exhibiting no overt morphological defects and maintaining the ability to reproduce (18). In this study, we focused on 4-7 dpf larval zebrafish as these timepoints are considered to be post-developmental for the acoustic startle circuit. It is possible that in zebrafish, as in mammals, the relevant circuits in *mecp2* mutant zebrafish undergo normal development before the onset of motor defects that are mild enough to allow survival in controlled laboratory environments. Behavioral analysis of juvenile and adult zebrafish *mecp2* mutants will test this hypothesis in future studies.

Zebrafish as a tool for unraveling mechanisms of MeCP2 function. Our transcriptomic data, together with previous proteomic analysis of larval and adult *mecp2* functions (75), demonstrate remarkable conservation of molecular pathways that depend on mecp2 function in zebrafish, mouse and RTT patients. Zebrafish offer a unique advantage for drug treatment studies, as compounds can be readily added to the media, making it a powerful tool for exploring candidate therapeutics. Recent work has demonstrated that regulators of MeCP2 stability can be targeted by drug treatment (76) and these compounds hold significant promise for exploration in the zebrafish model system. Furthermore, adult viability of *mecp2* mutant zebrafish allows behavioral analysis throughout their lifespan, enabling monitoring of progressive declines in motor responses. Collectively, these data provide compelling justification, and serve as a necessary foundation for future in-depth functional analyses of mecp2 in the zebrafish model. Ease of high-throughput behavioral and pharmacological analyses in the zebrafish model would complement and inform mouse studies, aiding in unraveling the complexities of MeCP2 function and designing therapeutic interventions for RTT and related neurodevelopmental disorders.

Methods

Generation and Maintenance of Zebrafish. Zebrafish (*Danio rerio*) were maintained according to established methods (77). The *mecp2*^{Q63X} line was obtained from Dr. Cecilia Moens via the Zebrafish International Resource Center (ZIRC). All experimental protocols using zebrafish were approved by the University of Wisconsin Animal Care and Use Committee and carried out in accordance with the institutional animal care protocols. Embryos were raised in E3 media at 28°C on a 14 hr/10 hr light/dark cycle through 7 dpf as previously described (78, 79). Embryos were generated from heterozygous crosses of adults carrying the *mecp2*^{Q63X} allele.

Genotyping. Genotyping of the *mecp2*^{Q63X} allele is based on the dCAPs assay (80) using the following primers:
mecp2^{Q63X} forward:
5'- ACAGCTGACTATAATACAGACCTGTCAAA -3'
and *mecp2*^{Q63X} reverse:
5'- TGGGTTCAGACTTCCCTGCCTCTGCCTGCA -3'.
To genotype the *mecp2*^{Q63X} allele, a mismatch SNP (marked in red) has been introduced into the reverse primer. During PCR, this mismatch creates a PstI (New England Biolabs, #R3140) restriction enzyme site in the amplified product derived from the wild-type DNA template. The PstI site is not present in the PCR product containing the *mecp2*^{Q63X} mutation.

Behavioral Analyses. On the day of behavioral testing, the larvae were held in 60mm-wide Petri dishes with 20 larvae in 10mL E3, kept on a white light box for at least 1 hour, and then transferred to a 4x4 (habituation), 6x6 grid (PPI) or 60mm dishes (gross movement, swim probability, turn probability, light flash, and dark flash). Acoustic startle behavior was elicited using an automated behavioral platform in which the intensity and timing of acoustic stimuli could be controlled (20, 39). Acoustic startle responses were elicited with a minishaker (Brüel & Kjær, Model 4810). The acoustic stimuli were of 3 ms duration, with 1000 Hz waveforms. Light offset-induced (dark flash) O-bends and light onset-induced (light flash) turns were elicited and analyzed as previously described (20, 39). Behavioral responses were captured at 1000 frames per second with a MotionPro Y4 video camera (Integrated Design Tools) with a 50 mm macro lens (Sigma Corporation of America) at 512 x 512 pixel resolution.

FLOTE was used to analyze startle responses in an experimenter-independent, automated manner (20). FLOTE tracked the position of individual larvae frame by frame and characterizes locomotor maneuvers (e.g. C-bend, O-bend, routine turn, swim, etc.) according to predefined kinematic parameters that distinguish these maneuvers. To evaluate habituation and measure startle responsiveness and kinematic parameters, 10 high-intensity stimuli were presented at non-habituating interstimulus intervals (ISIs) of 20 seconds followed by 30 high-intensity stimuli presented at 1.5 second ISIs. The degree to which larvae habituate was calculated as

previously defined (29, 39). To evaluate PPI, low and high stimuli were presented at a 300 ms ISI and the degree to which larvae demonstrate startle prepulse inhibition was calculated as previously defined (20). For habituation and PPI behavior, we report data representing the Mauthner neuron-dependent, short-latency C-bend startle (SLC) response. For kinematic analysis of ASRs, we report both SLCs and LLCs and their kinematic parameters. For light onset (light flash) responses, we report initiation of all turns and their kinematic parameters. For light offset (dark flash) responses, we report O-bends and their kinematic parameters.

RNA-Seq Transcriptome Analysis. Embryos derived from incrosses of *mecp2*^{Q63X} homozygous adults or wild-type adults were pooled in groups of three and processed for RNA extraction at 4 dpf as previously described (81). cDNA libraries were prepared using the TruSeq stranded mRNA library preparation protocol with poly-A selection and sequenced on the Illumina HiSeq. 2500. 10 biological replicates of each genotype, confirmed from raw sequencing data alignments using the Integrative Genomics Viewer, were analyzed.

Bioinformatic analysis of transcriptomic data adhere to recommended ENCODE guidelines and best practices for RNA-Seq (82). Alignment of adapter-trimmed (83) (Skewer v0.1.123) 2x150 (paired-end; PE) bp strand-specific Illumina reads to the *Danio rerio* GRCz11 genome (assembly accession GCF_000002035.6) was achieved with the Spliced Transcripts Alignment to a Reference (STAR v2.5.3a) software (84), a splice-junction aware aligner, using annotation modifications (v4.3.2) made by (85). Expression estimation was performed with RSEM v1.3.0 (RNASeq by Expectation Maximization) (86). To test for differential gene expression among individual group contrasts, expected read counts obtained from RSEM were used as input into edgeR (v3.16.5) (87). Inter-sample normalization was achieved among each pair of samples with trimmed mean of M-values (TMM) (88). Statistical significance of the negative-binomial regression test was adjusted with a Benjamini-Hochberg FDR correction at the 5% level (89). Prior to statistical analysis with edgeR, independent filtering was performed, requiring a threshold of at least 1 transcript count per million in at least 2 samples, ignoring any prior group assignment. The validity of the Benjamini-Hochberg FDR multiple testing procedure was evaluated by inspection of the uncorrected p-value distribution.

Expression Visualization and Gene Set Enrichment. A volcano plot was generated to depict the fold change and statistical significance of individual genes, with $\log_2$(Fold Change) by -$\log_{10}$(p-value) of individual genes shown as points and colorized by their significance and change in regulation (grey is non-significant, red is significant and upregulated, blue is significant and downregulated). The names of top 10 upregulated genes and top 10 downregulated genes by $\log_2$(Fold Change) were labeled (Fig. 3A).

Gene set enrichment analysis (GSEA) was performed using the clusterProfiler v4.6.2 R (90, 91) package. Gene sets were defined using the "drerio_gene_ensembl" dataset from Ensembl.org in the biomaRt v2.54.1 R package (92, 93). A scatterplot of significant gene sets was generated to show the change in expression of the top 40 sets, based on adj. p-value. This plot shows the BgRatio (the ratio of annotated genes) by gene set descriptor, points colored by the adjusted *p*-value, sized by count of genes in each set, and points shaped by the overall change (activated vs. suppressed) (Fig. 3B).

Both the scatterplot of differentially expressed gene sets and the volcano plot were rendered using the ggplot2 v3.4.2 R package (94).

Pathway Analysis. KEGG pathway analysis (42, 56) was performed using Pathways dre:00900, dre:00100, and dre:00140. These pathways were then colorized by relative gene expression using the pathview v1.38.0 R package (95) and overlaid on a manually redrawn pathway figure, combining the three individual pathways and showing only genes and portions of the pathways (genes and compounds) relevant to this study and species. Color bars on each gene node represent the relative gene expression of each sample in this study, scaled between [-1,1]. The top color bar of a given gene node represents the 10 wild-type samples and the bottom color bar represents the 10 mutant samples (Fig. 4).

Statistics. All graph generation and statistical analyses, including calculation of means, and SEM, were performed using GraphPad Prism software (www.graphpad.com). D'Agostino and Pearson normality test was used to test whether data were normally distributed. If data were normally distributed, significance was assessed using t-tests with Welch's correction or ANOVA with Dunnet's multiple comparisons test. If data were not normally distributed, Mann-Whitney test or Kruskall-Wallis test with Dunn's multiple comparisons test was used. *p*-values below 0.05 were considered statistically significant.

Author Contributions

Nicholas J. Santistevan: Conceptualization, Methodology, Validation, Formal Analysis, Investigation, Data Curation, Visualization, Writing - Original Draft, Writing - Reviewing and Editing, Funding Acquisition. **Colby T. Ford:** Software, Formal Analysis, Resources, Data Curation, Visualization, Writing - Reviewing and Editing. **Cole S. Gilsdorf:** Investigation, Writing - Reviewing and Editing. **Yevgenya Grinblat:** Writing - Original Draft, Writing - Reviewing and Editing, Supervision, Project Administration, Funding Acquisition.

Acknowledgements

We thank the members of the Grinblat lab for technical support and zebrafish line maintenance, and members of the labs of Dr. Mary Halloran, Dr. Katie Drerup, and Dr. David Ehrlich for help with zebrafish line maintenance. We thank Dr. Cecilia Moens for providing the *mecp2*^{Q63X} mutant

zebrafish line and Dr. Xinyu Zhao for expert insight and valuable advice. This work was funded by grants from the University of Wisconsin-Madison (Science and Medicine Graduate Research fellowship to N.J.S., Department of Integrative Biology funding to N.J.S, and the Office of the Vice Chancellor for Research and Graduate Education/Wisconsin Alumni Research Foundation to N.J.S. and Y. G), and by the National Science Foundation Graduate Research Fellowship Program under Grant Numbers DGE-1256259 and DGE-1747503 to N.J.S. Any opinions, findings, and conclusions or recommendations expressed in this material are those of the authors and do not necessarily reflect the views of the National Science Foundation.

Data availability statement

All code, data, results, and additional analyses are openly available on GitHub at:
https://github.com/colbyford/zebrafish_mecp2_expression.
These data include RNA-seq gene expression values, gene set enrichment results, figure generation and statistics code, and additional pathway analyses.

Funding statement

This work was funded by grants from the University of Wisconsin-Madison (Science and Medicine Graduate Research fellowship to N.J.S., Department of Integrative Biology funding to N.J.S, and the Office of the Vice Chancellor for Research and Graduate Education/Wisconsin Alumni Research Foundation to N.J.S. and Y. G), and by the National Science Foundation Graduate Research Fellowship Program under Grant Numbers DGE-1256259 and DGE-1747503 to N.J.S. Any opinions, findings, and conclusions or recommendations expressed in this material are those of the authors and do not necessarily reflect the views of the National Science Foundation.

Conflict of interest disclosure

The authors have declared that no competing interests exist.

Ethics approval statement

All experiments and animal protocols were approved and conducted in accordance with the University of Wisconsin Institutional Animal Care and Use Committee (IACUC).

Patient consent statement

Not applicable

Permission to reproduce material from other sources

Not applicable

Clinical trial registration

Not applicable

Bibliography

1. Regina M. Carney, Chantelle M. Wolpert, Sarah A. Ravan, Mona Shahbazian, Allison Ashley-Koch, Michael L. Cuccaro, Jeffery M. Vance, and Margaret A. Pericak-Vance. Identification of MeCP2 mutations in a series of females with autistic disorder. *Pediatric Neurology*, 28(3):205–211, mar 2003. doi: 10.1016/s0887-8994(02)00624-0.
2. DAVID COHEN, GABRIELA LAZAR, PHILIPPE COUVERT, VINCENT DESPORTES, DIDIER LIPPE, PHILIPPE MAZET, and DELPHINE HÉRON. Mecp2 mutation in a boy with language disorder and schizophrenia. *American Journal of Psychiatry*, 159(1):148–a–149, jan 2002. doi: 10.1176/appi.ajp.159.1.148-a.
3. Akane Shibayama, Edwin H. Cook, Jinong Feng, Cecile Glanzmann, Jin Yan, Nick Craddock, Ian R. Jones, David Goldman, Leonard L. Heston, and Steve S. Sommer. MECP2 structural and 3?-UTR variants in schizophrenia, autism and other psychiatric diseases: A possible association with autism. *American Journal of Medical Genetics*, 128B(1):50–53, 2004. doi: 10.1002/ajmg.b.30016.
4. Ruthie E. Amir, Ignatia B. Van den Veyver, Mimi Wan, Charles Q. Tran, Uta Francke, and Huda Y. Zoghbi. Rett syndrome is caused by mutations in x-linked MECP2, encoding methyl-CpG-binding protein 2. *Nature Genetics*, 23(2):185–188, oct 1999. doi: 10.1038/13810.
5. Maria Chahrour and Huda Y. Zoghbi. The story of rett syndrome: From clinic to neurobiology. *Neuron*, 56(3):422–437, nov 2007. doi: 10.1016/j.neuron.2007.10.001.
6. Bengt Hagberg, Jean Aicardi, Karin Dias, and Ovidio Ramos. A progressive syndrome of autism, dementia, ataxia, and loss of purposeful hand use in girls: Rett's syndrome: Report of 35 cases. *Annals of Neurology*, 14(4):471–479, oct 1983. doi: 10.1002/ana.410140412.
7. Dawna Duncan Armstrong. Neuropathology of rett syndrome. *Journal of Child Neurology*, 20(9):747–753, sep 2005. doi: 10.1177/08830738050200090901.
8. Louise E. Coverdale, Christopher J. Martyniuk, Vance L. Trudeau, and C. Cristofre Martin. Differential expression of the methyl-cytosine binding protein 2 gene in embryonic and adult brain of zebrafish. *Developmental Brain Research*, 153(2):281–287, nov 2004. doi: 10.1016/j.devbrainres.2004.08.009.
9. Richard D. Smrt, Julialea Eaves-Egenes, Basam Z. Barkho, Nicholas J. Santistevan, Chunmei Zhao, James B. Aimone, Fred H. Gage, and Xinyu Zhao. Mecp2 deficiency leads to delayed maturation and altered gene expression in hippocampal neurons. *Neurobiology of Disease*, 27(1):77–89, jul 2007. doi: 10.1016/j.nbd.2007.04.005.
10. Yi Sun, Yu Gao, Joseph J Tidei, Minjie Shen, Johnson T Hoang, Daniel F Wagner, and Xinyu Zhao. Loss of MeCP2 in immature neurons leads to impaired network integration. *Human Molecular Genetics*, 28(2):245–257, oct 2018. doi: 10.1093/hmg/ddy338.
11. Hsiao-Tuan Chao, Hongmei Chen, Rodney C. Samaco, Mingshan Xue, Maria Chahrour, Jong Yoo, Jeffrey L. Neul, Shiaoching Gong, Hui-Chen Lu, Nathaniel Heintz, Marc Ekker, John L. R. Rubenstein, Jeffrey L. Noebels, Christian Rosenmund, and Huda Y. Zoghbi. Dysfunction in GABA signalling mediates autism-like stereotypies and rett syndrome phenotypes. *Nature*, 468(7321):263–269, nov 2010. doi: 10.1038/nature09582.
12. Chao-Yin Chen, Jacopo Di Lucente, Yen-Chu Lin, Cheng-Chang Lien, Michael A. Rogawski, Izumi Maezawa, and Lee-Way Jin. Defective GABAergic neurotransmission in the nucleus tractus solitarius in mecp2-null mice, a model of rett syndrome. *Neurobiology of Disease*, 109:25–32, jan 2018. doi: 10.1016/j.nbd.2017.09.006.
13. Sharyl L. Fyffe, Jeff L. Neul, Rodney C. Samaco, Hsiao-Tuan Chao, Shay Ben-Shachar, Paolo Moretti, Bryan E. McGill, Evan H. Goulding, Elinor Sullivan, Laurence H. Tecott, and Huda Y. Zoghbi. Deletion of mecp2 in sim1-expressing neurons reveals a critical role for MeCP2 in feeding behavior, aggression, and the response to stress. *Neuron*, 59(6):947–958, sep 2008. doi: 10.1016/j.neuron.2008.07.030.
14. Terry Gemelli, Olivier Berton, Erika D. Nelson, Linda I. Perrotti, Rudolf Jaenisch, and Lisa M. Monteggia. Postnatal loss of methyl-CpG binding protein 2 in the forebrain is sufficient to mediate behavioral aspects of rett syndrome in mice. *Biological Psychiatry*, 59(5):468–476, mar 2006. doi: 10.1016/j.biopsych.2005.07.025.
15. Jacky Guy, Brian Hendrich, Megan Holmes, Joanne E. Martin, and Adrian Bird. A mouse mecp2-null mutation causes neurological symptoms that mimic rett syndrome. *Nature Genetics*, 27(3):322–326, mar 2001. doi: 10.1038/85899.
16. Laura Marie Lombardi, Steven Andrew Baker, and Huda Yahya Zoghbi. MECP2 disorders: from the clinic to mice and back. *Journal of Clinical Investigation*, 125(8):2914–2923, aug 2015. doi: 10.1172/jci78167.
17. R. C. Samaco, J. D. Fryer, J. Ren, S. Fyffe, H.-T. Chao, Y. Sun, J. J. Greer, H. Y. Zoghbi, and J. L. Neul. A partial loss of function allele of methyl-CpG-binding protein 2 predicts a human neurodevelopmental syndrome. *Human Molecular Genetics*, 17(12):1718–1727, mar 2008. doi: 10.1093/hmg/ddn062.
18. Thomas Pietri, Angel-Carlos Roman, Nicolas Guyon, Sebastián A. Romano, Philip Washbourne, Cecilia B. Moens, Gonzalo G. de Polavieja, and Germán Sumbre. The first mecp2-null zebrafish model shows altered motor behaviors. *Frontiers in Neural Circuits*, 7, 2013. doi: 10.3389/fncir.2013.00118.
19. Keisuke Nozawa, Yanbin Lin, Ryota Kubodera, Yuki Shimizu, Hideomi Tanaka, and Toshio Ohshima. Zebrafish mecp2 is required for proper axonal elongation of motor neurons and synapse formation. *Developmental Neurobiology*, 77(9):1101–1113, apr 2017. doi: 10.1002/dneu.22498.
20. Harold A. Burgess and Michael Granato. Sensorimotor gating in larval zebrafish. *The Journal of Neuroscience*, 27(18):4984–4994, may 2007. doi: 10.1523/jneurosci.0615-07.2007.
21. Yohaan Fernandes, Mindy Rampersad, Emma M. Jones, and Johann K. Eberhart. Social deficits following embryonic ethanol exposure arise in post-larval zebrafish. *Addiction Biology*, 24(5):898–907, sep 2018. doi: 10.1111/adb.12649.
22. Friederike Ehrhart, Susan L. M. Coort, Elisa Cirillo, Eric Smeets, Chris T. Evelo, and Leopold M. G. Curfs. Rett syndrome – biological pathways leading from MECP2 to disorder phenotypes. *Orphanet Journal of Rare Diseases*, 11(1), nov 2016. doi: 10.1186/s13023-016-0545-5.
23. Patricia M. Horvath and Lisa M. Monteggia. MeCP2 as an activator of gene expression. *Trends in Neurosciences*, 41(2):72–74, feb 2018. doi: 10.1016/j.tins.2017.11.005.
24. Lauren L. Orefice, Amanda L. Zimmerman, Anda M. Chirila, Steven J. Sleboda, Joshua P.

Head, and David D. Ginty. Peripheral mechanosensory neuron dysfunction underlies tactile and behavioral deficits in mouse models of ASDs. *Cell*, 166(2):299–313, jul 2016. doi: 10.1016/j.cell.2016.05.033.

25. Harold A. Burgess and Michael Granato. Modulation of locomotor activity in larval zebrafish during light adaptation. *Journal of Experimental Biology*, 210(14):2526–2539, jul 2007. doi: 10.1242/jeb.003939.
26. Henri Korn and Donald S. Faber. The mauthner cell half a century later: A neurobiological model for decision-making? *Neuron*, 47(1):13–28, jul 2005. doi: 10.1016/j.neuron.2005.05.019.
27. Cong Yao, Kimberly G. Vanderpool, Matthew Delfiner, Vanessa Eddy, Alexander G. Lucaci, Carolina Soto-Riveros, Thomas Yasumura, John E. Rash, and Alberto E. Pereda. Electrical synaptic transmission in developing zebrafish: properties and molecular composition of gap junctions at a central auditory synapse. *Journal of Neurophysiology*, 112(9):2102–2113, nov 2014. doi: 10.1152/jn.00397.2014.
28. Henri Korn, A. Triller, and Donald S. Faber. Structural correlates of recurrent collateral interneurons producing both electrical and chemical inhibitions of the mauthner cell. *Proceedings of the Royal Society of London. Series B. Biological Sciences*, 202(1149):533–538, sep 1978. doi: 10.1098/rspb.1978.0085.
29. Nicholas J. Santistevan, Jessica C. Nelson, Elelbin A. Ortiz, Andrew H. Miller, Dima Kenj Halabi, Zoë A. Sippl, Michael Granato, and Yevgenya Grinblat. cacna2d3, a voltage-gated calcium channel subunit, functions in vertebrate habituation learning and the startle sensitivity threshold. *PLOS ONE*, 17(7):e0270903, jul 2022. doi: 10.1371/journal.pone.0270903.
30. Marc A. Wolman, Roshan A. Jain, Kurt C. Marsden, Hannah Bell, Julianne Skinner, Katharina E. Hayer, John B. Hogenesch, and Michael Granato. A genome-wide screen identifies PAPP-AA-mediated IGFR signaling as a novel regulator of habituation learning. *Neuron*, 85 (6):1200–1211, mar 2015. doi: 10.1016/j.neuron.2015.02.025.
31. Philip M. Groves and Richard F. Thompson. Habituation: A dual-process theory. *Psychological Review*, 77(5):419–450, sep 1970. doi: 10.1037/h0029810.
32. Susan B. Powell, Martin Weber, and Mark A. Geyer. Genetic models of sensorimotor gating: Relevance to neuropsychiatric disorders. In *Current Topics in Behavioral Neurosciences*, pages 251–318. Springer Berlin Heidelberg, 2011. doi: 10.1007/7854_2011_195.
33. David L. Braff, Mark A. Geyer, and Neal R. Swerdlow. Human studies of prepulse inhibition of startle: normal subjects, patient groups, and pharmacological studies. *Psychopharmacology*, 156(2-3):234–258, jun 2001. doi: 10.1007/s002130100810.
34. David L. Braff. Sensorimotor gating and schizophrenia. *Archives of General Psychiatry*, 47 (2):181, feb 1990. doi: 10.1001/archpsyc.1990.01810140081011.
35. Severine Durand, Annarita Patrizi, Kathleen B. Quast, Lea Hachigian, Roman Pavlyuk, Alka Saxena, Piero Carninci, Takao K. Hensch, and Michela Fagiolini. NMDA receptor regulation prevents regression of visual cortical function in the absence of mecp2. *Neuron*, 76(6): 1078–1090, dec 2012. doi: 10.1016/j.neuron.2012.12.004.
36. Jocelyn J. LeBlanc, Geneva DeGregorio, Eleonora Centofante, Vanessa K. Vogel-Farley, Katherine Barnes, Walter E. Kaufmann, Michela Fagiolini, and Charles A. Nelson. Visual evoked potentials detect cortical processing deficits in rett syndrome. *Annals of Neurology*, 78(5):775–786, sep 2015. doi: 10.1002/ana.24513.
37. Ling jie He, Nan Liu, Tian lin Cheng, Xiao jing Chen, Yi ding Li, You sheng Shu, Zi long Qiu, and Xiao hui Zhang. Conditional deletion of mecp2 in parvalbumin-expressing GABAergic cells results in the absence of critical period plasticity. *Nature Communications*, 5(1), oct 2014. doi: 10.1038/ncomms6036.
38. Andrew H. Miller, Hollis B. Howe, Bryan M. Krause, Scott A. Friedle, Matthew I. Banks, Brian D. Perkins, and Marc A. Wolman. Pregnancy-associated plasma protein-aa regulates photoreceptor synaptic development to mediate visually guided behavior. *The Journal of Neuroscience*, 38(22):5220–5236, may 2018. doi: 10.1523/jneurosci.0061-18.2018.
39. Marc A. Wolman, Roshan A. Jain, Laura Liss, and Michael Granato. Chemical modulation of memory formation in larval zebrafish. *Proceedings of the National Academy of Sciences*, 108(37):15468–15473, aug 2011. doi: 10.1073/pnas.1107156108.
40. Jing-Wen Lyu, Bo Yuan, Tian-Lin Cheng, Zi-Long Qiu, and Wen-Hao Zhou. Reciprocal regulation of autism-related genes MeCP2 and PTEN via microRNAs. *Scientific Reports*, 6 (1), feb 2016. doi: 10.1038/srep20392.
41. Maria Chahrour, Sung Yun Jung, Chad Shaw, Xiaobo Zhou, Stephen T. C. Wong, Jun Qin, and Huda Y. Zoghbi. MeCP2, a key contributor to neurological disease, activates and represses transcription. *Science*, 320(5880):1224–1229, may 2008. doi: 10.1126/science.1153252.
42. M. Kanehisa. KEGG: Kyoto encyclopedia of genes and genomes. *Nucleic Acids Research*, 28(1):27–30, jan 2000. doi: 10.1093/nar/28.1.27.
43. Qingping Zhang, Xiaoxu Yang, Jiaping Wang, Jiarui Li, Qixi Wu, Yongxin Wen, Ying Zhao, Xiaoying Zhang, He Yao, Xiru Wu, Shujie Yu, Liping Wei, and Xinhua Bao. Genomic mosaicism in the pathogenesis and inheritance of a rett syndrome cohort. *Genetics in Medicine*, 21(6):1330–1338, jun 2019. doi: 10.1038/s41436-018-0348-2.
44. Hai Zeng, Sisi Zhao, Zhao Pang, Shiqi Wang, Luxi Cao, and Yimin Zhang. Identification of key genes and pathways in the hippocampus after traumatic brain injury: Bioinformatics analysis and experimental validation. *Journal of Integrative Neuroscience*, 22(2):44, feb 2023. doi: 10.31083/j.jin2202044.
45. Gabor Nagy and Susan L Ackerman. Cholesterol metabolism and rett syndrome pathogenesis. *Nature Genetics*, 45(9):965–967, aug 2013. doi: 10.1038/ng.2738.
46. Marco Segatto, Laura Trapani, Ilenia Di Tunno, Claudia Sticozzi, Giuseppe Valacchi, Joussef Hayek, and Valentina Pallottini. Cholesterol metabolism is altered in rett syndrome: A study on plasma and primary cultured fibroblasts derived from patients. *PLoS ONE*, 9(8):e104834, aug 2014. doi: 10.1371/journal.pone.0104834.
47. Holly Brunton, Aaron A. Goodarzi, Angela T. Noon, Amruta Shrikhande, R. Scott Hansen, Penny A. Jeggo, and Atsushi Shibata. Analysis of human syndromes with disordered chromatin reveals the impact of heterochromatin on the efficacy of atm-dependent g2/m checkpoint arrest. *Molecular and Cellular Biology*, 31(19):4022–4035, oct 2011. doi: 10.1128/mcb.05289-11.
48. L M Julian, Y Liu, C A Pakenham, D Dugal-Tessier, V Ruzhynsky, S Bae, S-Y Tsai, G Leone, R S Slack, and A Blais. Tissue-specific targeting of cell fate regulatory genes by e2f factors. *Cell Death & Differentiation*, 23(4):565–575, apr 2015. doi: 10.1038/cdd.2015.36.
49. Anna Bergo, Marta Strollo, Marta Gai, Isabella Barbiero, Gilda Stefanelli, Sarah Sertic, Clementina Cobolli Gigli, Ferdinando Di Cunto, Charlotte Kilstrup-Nielsen, and Nicoletta Landsberger. Methyl-CpG binding protein 2 (MeCP2) localizes at the centrosome and is required for proper mitotic spindle organization. *Journal of Biological Chemistry*, 290(6): 3223–3237, feb 2015. doi: 10.1074/jbc.m114.608125.
50. Christie M Buchovecky, Stephen D Turley, Hannah M Brown, Stephanie M Kyle, Jeffrey G McDonald, Benny Liu, Andrew A Pieper, Wenhui Huang, David M Katz, David W Russell, Jay Shendure, and Monica J Justice. A suppressor screen in mecp2 mutant mice implicates cholesterol metabolism in rett syndrome. *Nature Genetics*, 45(9):1013–1020, jul 2013. doi: 10.1038/ng.2714.
51. Valerie Matagne, Emilie Borloz, Yann Ehinger, Lydia Saidi, Laurent Villard, and Jean-Christophe Roux. Severe offtarget effects following intravenous delivery of AAV9-MECP2 in a female mouse model of rett syndrome. *Neurobiology of Disease*, 149:105235, feb 2021. doi: 10.1016/j.nbd.2020.105235.
52. D Bernard, J Gil, P Dumont, S Rizzo, D Monté, B Quatannens, D Hudson, T Visakorpi, F Fuks, and Y de Launoit. The methyl-CpG-binding protein MECP2 is required for prostate cancer cell growth. *Oncogene*, 25(9):1358–1366, dec 2005. doi: 10.1038/sj.onc.1209179.
53. Sampathkumar Rangasamy, Shannon Olfers, Brittany Gerald, Alex Hilbert, Sean Svejda, and Vinodh Narayanan. Reduced neuronal size and mTOR pathway activity in the mecp2 a140v rett syndrome mouse model. *F1000Research*, 5:2269, sep 2016. doi: 10.12688/f1000research.8156.1.
54. Joseph L. Goldstein and Michael S. Brown. Regulation of the mevalonate pathway. *Nature*, 343(6257):425–430, feb 1990. doi: 10.1038/343425a0.
55. David W. Russell. The enzymes, regulation, and genetics of bile acid synthesis. *Annual Review of Biochemistry*, 72(1):137–174, jun 2003. doi: 10.1146/annurev.biochem.72.121801.161712.
56. Minoru Kanehisa, Miho Furumichi, Yoko Sato, Masayuki Kawashima, and Mari Ishiguro-Watanabe. KEGG for taxonomy-based analysis of pathways and genomes. *Nucleic Acids Research*, 51(D1):D587–D592, oct 2022. doi: 10.1093/nar/gkac963.
57. Rodney C. Samaco, Christopher M. McGraw, Christopher S. Ward, Yaling Sun, Jeffrey L. Neul, and Huda Y. Zoghbi. Female mecp2 +/- mice display robust behavioral deficits on two different genetic backgrounds providing a framework for pre-clinical studies. *Human Molecular Genetics*, 22(1):96–109, oct 2012. doi: 10.1093/hmg/dds406.
58. Richard Z. Chen, Schahram Akbarian, Matthew Tudor, and Rudolf Jaenisch. Deficiency of methyl-CpG binding protein-2 in CNS neurons results in a rett-like phenotype in mice. *Nature Genetics*, 27(3):327–331, mar 2001. doi: 10.1038/85906.
59. Gregory J. Pelka, Catherine M. Watson, Tania Radziewic, Melinda Hayward, Hooshang Lahooti, John Christodoulou, and Patrick P. L. Tam. Mecp2 deficiency is associated with learning and cognitive deficits and altered gene activity in the hippocampal region of mice. *Brain*, 129(4):887–898, feb 2006. doi: 10.1093/brain/awl022.
60. Juan E Belforte, Veronika Zsiros, Elyse R Sklar, Zhihong Jiang, Gu Yu, Yuqing Li, Elizabeth M Quinlan, and Kazu Nakazawa. Postnatal NMDA receptor ablation in corticolimbic interneurons confers schizophrenia-like phenotypes. *Nature Neuroscience*, 13(1):76–83, nov 2009. doi: 10.1038/nn.2447.
61. Vardhan S. Dani, Qiang Chang, Arianna Maffei, Gina G. Turrigiano, Rudolf Jaenisch, and Sacha B. Nelson. Reduced cortical activity due to a shift in the balance between excitation and inhibition in a mouse model of rett syndrome. *Proceedings of the National Academy of Sciences*, 102(35):12560–12565, aug 2005. doi: 10.1073/pnas.0506071102.
62. Nadine Gogolla, Jocelyn J. LeBlanc, Kathleen B. Quast, Thomas C. Südhof, Michela Fagiolini, and Takao K. Hensch. Common circuit defect of excitatory-inhibitory balance in mouse models of autism. *Journal of Neurodevelopmental Disorders*, 1(2):172–181, jun 2009. doi: 10.1007/s11689-009-9023-x.
63. J. L. R. Rubenstein and M. M. Merzenich. Model of autism: increased ratio of excitation/inhibition in key neural systems. *Genes, Brain and Behavior*, 2(5):255–267, oct 2003. doi: 10.1034/j.1601-183x.2003.00037.x.
64. Neal R Swerdlow, David L Braff, and Mark A Geyer. Sensorimotor gating of the startle reflex: what we said 25 years ago, what has happened since then, and what comes next. *Journal of Psychopharmacology*, 30(11):1072–1081, aug 2016. doi: 10.1177/0269881116661075.
65. Xiangling Meng, Wei Wang, Hui Lu, Ling jie He, Wu Chen, Eugene S Chao, Marta L Fiorotto, Bin Tang, Jose A Herrera, Michelle L Seymour, Jeffrey L Neul, Fred A Pereira, Jianrong Tang, Mingshan Xue, and Huda Y Zoghbi. Manipulations of MeCP2 in glutamatergic neurons highlight their contributions to rett and other neurological disorders. *eLife*, 5, jun 2016. doi: 10.7554/elife.14199.
66. Bridget Valsamis and Susanne Schmid. Habituation and prepulse inhibition of acoustic startle in rodents. *Journal of Visualized Experiments*, 55(e3446), sep 2011. doi: 10.3791/3446.
67. Charles B. Kimmel, Jill Patterson, and Richard O. Kimmel. The development and behavioral characteristics of the startle response in the zebra fish. *Developmental Psychobiology*, 7 (1):47–60, jan 1974. doi: 10.1002/dev.420070109.
68. Stephen Tetzchner, Karl H Jacobsen, Lars Smith, Ola H Skjeldal, Arvid Heiberg, and Joseph F Fagan. Vision, cognition, and devleopmental characteristics of girls and women with rhett syndrome. *Developmental Medicine & Child Neurology*, 38(3):212–225, nov 2008. doi: 10.1111/j.1469-8749.1996.tb15083.x.
69. Heinz Wässle. Parallel processing in the mammalian retina. *Nature Reviews Neuroscience*, 5(10):747–757, oct 2004. doi: 10.1038/nrn1497.
70. Daniela Tropea, Emanuela Giacometti, Nathan R. Wilson, Caroline Beard, Cortina McCurry, Dong Dong Fu, Ruth Flannery, Rudolf Jaenisch, and Mriganka Sur. Partial reversal of rett syndrome-like symptoms in MeCP2 mutant mice. *Proceedings of the National Academy of Sciences*, 106(6):2029–2034, feb 2009. doi: 10.1073/pnas.0812394106.
71. Zhe-Feng Yuan, Shan-Shan Mao, Jue Shen, Li-Hua Jiang, Lu Xu, Jia-Lu Xu, and Feng Gao. Insulin-like growth factor-1 down-regulates the phosphorylation of FXYD1 and rescues behavioral deficits in a mouse model of rett syndrome. *Frontiers in Neuroscience*, 14, jan 2020. doi: 10.3389/fnins.2020.00020.
72. M. van der Vaart, O. Svoboda, B. G. Weijts, R. Espín-Palazón, V. Sapp, T. Pietri, M. Bagnat, A. R. Muotri, and D. Traver. Mecp2 regulates tnfa during zebrafish embryonic development and acute inflammation. *Disease Models & Mechanisms*, jan 2017. doi: 10.1242/dmm.

026922.
73. Mohamed A. El-Brolosy, Zacharias Kontarakis, Andrea Rossi, Carsten Kuenne, Stefan Günther, Nana Fukuda, Khrievono Kikhi, Giulia L. M. Boezio, Carter M. Takacs, Shih-Lei Lai, Ryuichi Fukuda, Claudia Gerri, Antonio J. Giraldez, and Didier Y. R. Stainier. Genetic compensation triggered by mutant mRNA degradation. *Nature*, 568(7751):193–197, apr 2019. doi: 10.1038/s41586-019-1064-z.
74. Andrea Rossi, Zacharias Kontarakis, Claudia Gerri, Hendrik Nolte, Soraya Hölper, Marcus Krüger, and Didier Y. R. Stainier. Genetic compensation induced by deleterious mutations but not gene knockdowns. *Nature*, 524(7564):230–233, jul 2015. doi: 10.1038/nature14580.
75. Alessio Cortelazzo, Thomas Pietri, Claudio De Felice, Silvia Leoncini, Roberto Guerranti, Cinzia Signorini, Anna Maria Timperio, Lello Zolla, Lucia Ciccoli, and Joussef Hayek. Proteomic analysis of the rett syndrome experimental model mecp2q63x mutant zebrafish. *Journal of Proteomics*, 154:128–133, feb 2017. doi: 10.1016/j.jprot.2016.12.010.
76. Laura M. Lombardi, Manar Zaghlula, Yehezkel Sztainberg, Steven A. Baker, Tiemo J. Klisch, Amy A. Tang, Eric J. Huang, and Huda Y. Zoghbi. An RNA interference screen identifies druggable regulators of MeCP2 stability. *Science Translational Medicine*, 9(404), aug 2017. doi: 10.1126/scitranslmed.aaf7588.
77. Monte Westerfield. *The Zebrafish Book; A Guide for the Laboratory Use of Zebrafish (Brachydanio rerio)*. University of Oregon Press, Eugene, OR, 2nd edition, 1993.
78. Michael Gyda, Marc Wolman, Kristin Lorent, and Michael Granato. The tumor suppressor gene retinoblastoma-1 is required for retinotectal development and visual function in zebrafish. *PLoS Genetics*, 8(11):e1003106, nov 2012. doi: 10.1371/journal.pgen.1003106.
79. Charles B. Kimmel, William W. Ballard, Seth R. Kimmel, Bonnie Ullmann, and Thomas F. Schilling. Stages of embryonic development of the zebrafish. *Developmental Dynamics*, 203(3):253–310, jul 1995. doi: 10.1002/aja.1002030302.
80. Michael M Neff, Edward Turk, and Michael Kalishman. Web-based primer design for single nucleotide polymorphism analysis. *Trends in Genetics*, 18(12):613–615, dec 2002. doi: 10.1016/s0168-9525(02)02820-2.
81. Baul Yoon, Pan Yeung, Nicholas Santistevan, Lauren E. Bluhm, Kenta Kawasaki, Janina Kueper, Richard Dubielzig, Jennifer VanOudenhove, Justin Cotney, Eric C. Liao, and Yevgenya Grinblat. Zebrafish models of alx-linked frontonasal dysplasia reveal a role for alx1 and alx3 in the anterior segment and vasculature of the developing eye. *Biology Open*, 11(5), may 2022. doi: 10.1242/bio.059189.
82. The ENCODE Project Consortium. An integrated encyclopedia of dna elements in the human genome. *Nature*, 489(7414):57–74, Sep 2012. ISSN 1476-4687. doi: 10.1038/nature11247.
83. Hongshan Jiang, Rong Lei, Shou-Wei Ding, and Shuifang Zhu. Skewer: a fast and accurate adapter trimmer for next-generation sequencing paired-end reads. *BMC Bioinformatics*, 15 (1):182, Jun 2014. ISSN 1471-2105. doi: 10.1186/1471-2105-15-182.
84. Alexander Dobin, Carrie A. Davis, Felix Schlesinger, Jorg Drenkow, Chris Zaleski, Sonali Jha, Philippe Batut, Mark Chaisson, and Thomas R. Gingeras. STAR: ultrafast universal RNA-seq aligner. *Bioinformatics*, 29(1):15–21, oct 2012. doi: 10.1093/bioinformatics/bts635.
85. Nathan D Lawson, Rui Li, Masahiro Shin, Ann Grosse, Onur Yukselen, Oliver A Stone, Alper Kucukural, and Lihua Zhu. An improved zebrafish transcriptome annotation for sensitive and comprehensive detection of cell type-specific genes. *eLife*, 9, aug 2020. doi: 10.7554/elife.55792.
86. Bo Li and Colin N Dewey. RSEM: accurate transcript quantification from RNA-seq data with or without a reference genome. *BMC Bioinformatics*, 12(1), aug 2011. doi: 10.1186/1471-2105-12-323.
87. Mark D. Robinson, Davis J. McCarthy, and Gordon K. Smyth. edger: a bioconductor package for differential expression analysis of digital gene expression data. *Bioinformatics*, 26 (1):139–140, nov 2009. doi: 10.1093/bioinformatics/btp616.
88. Mark D Robinson and Alicia Oshlack. A scaling normalization method for differential expression analysis of RNA-seq data. *Genome Biology*, 11(3):R25, 2010. doi: 10.1186/gb-2010-11-3-r25.
89. Anat Reiner, Daniel Yekutieli, and Yoav Benjamini. Identifying differentially expressed genes using false discovery rate controlling procedures. *Bioinformatics*, 19(3):368–375, feb 2003. doi: 10.1093/bioinformatics/btf877.
90. Tianzhi Wu, Erqiang Hu, Shuangbin Xu, Meijun Chen, Pingfan Guo, Zehan Dai, Tingze Feng, Lang Zhou, Wenli Tang, Li Zhan, Xiaocong Fu, Shanshan Liu, Xiaochen Bo, and Guangchuang Yu. clusterprofiler 4.0: A universal enrichment tool for interpreting omics data. *The Innovation*, 2(3), Aug 2021. ISSN 2666-6758. doi: 10.1016/j.xinn.2021.100141.
91. Guangchuang Yu, Li-Gen Wang, Yanyan Han, and Qing-Yu He. clusterprofiler: an r package for comparing biological themes among gene clusters. *OMICS: A Journal of Integrative Biology*, 16(5):284–287, 2012. doi: 10.1089/omi.2011.0118. PMID: 22455463.
92. S. Durinck, Y. Moreau, A. Kasprzyk, S. Davis, B. De Moor, A. Brazma, and W. Huber. BioMart and bioconductor: a powerful link between biological databases and microarray data analysis. *Bioinformatics*, 21(16):3439–3440, aug 2005. doi: 10.1093/bioinformatics/bti525.
93. Steffen Durinck, Paul T Spellman, Ewan Birney, and Wolfgang Huber. Mapping identifiers for the integration of genomic datasets with the r/bioconductor package biomaRt. *Nature Protocols*, 4(8):1184–1191, jul 2009. doi: 10.1038/nprot.2009.97.
94. Hadley Wickham. *ggplot2*. Springer International Publishing, 2016. doi: 10.1007/978-3-319-24277-4.
95. Weijun Luo and Cory Brouwer. Pathview: an r/bioconductor package for pathway-based data integration and visualization. *Bioinformatics*, 29(14):1830–1831, jun 2013. doi: 10.1093/bioinformatics/btt285.